PMMA-doped CdSe quantum dots as saturable absorber in a *Q*-switched all-fiber laser

M. B. Hisyam[1], M. F. Rusdi[1], A. A. Latiff[2], and S. W. Harun[1,2,*]

[1]*Department of Electrical Engineering, Faculty of Engineering, University of Malaya, Kuala Lumpur 50603, Malaysia*
[2]*Photonics Research Center, University of Malaya, Kuala Lumpur 50603, Malaysia*
**Corresponding author: swharun@um.edu.my*

Received April 23, 2016; accepted June 14, 2016; posted online July 25, 2016

We demonstrate the generation of *Q*-switched pulses from an ytterbium-doped fiber laser (YDFL) using quantum dot (QD) CdSe as a passive saturable absorber (SA). The CdSe QD is fabricated by the synthesis of CdO, Se, and manganese acetate and paraffin oil and oleic acid as the solvent and surfactant, respectively. The CdSe QD is then doped into poly-methyl-methacrylate (PMMA) via an emulsion polymerization process. A PMMA-hosted CdSe QD thin flake with a homogeneous end surface is then formed and placed between two ferrules and assembled in a YDFL cavity to achieve the *Q*-switching operation with a repetition rate of 24.45 to 40.50 kHz while varying the pump power from 975 to 1196 mW. The pulse width changes from 6.78 to 3.65 μs with a maximum calculated pulse energy at 0.77 μJ at a pump power of 1101 mW. This work may be the first demonstration of CdSe QD-based *Q*-switching in an all-fiber configuration that should give proportional insight into semiconductor QD materials in photonics applications.

OCIS codes: 140.3540, 140.3510, 140.3615, 160.4236.
doi: 10.3788/COL201614.081404.

Fiber lasers have been extensively developed since they were proven to have great potential over other type of lasers, such as dye, gas, chemical, solid state, and semiconductor. They are used in various applications, including pulsed laser systems, which have been widely used in telecommunications, bio-sensing, medicine, imaging, range finding, and material processing[1–3]. One of the main technique is the *Q*-switched pulsed fiber laser, which can be achieved by either active or passive modes. In general, passive mode is desirable since it eliminates the involvement of electro-mechanical components and is able to achieve a much higher frequency. Several ways have been discovered to achieve stable passive *Q*-switching operations, including the induction of an artificial saturable absorber (SA) by utilizing the non-linear polarization rotation effect, a non-linear optical loop mirror, and a non-linear amplifying loop mirror. The other method is by using a real SA, such as an ion-doped crystal[4,5], a bleachable dye, or a semiconductor saturable absorber mirror (SESAM)[6]. However, the SESAM is expensive and has a very narrow operation bandwidth and thus a lower optical response even though it is the most mature of the commercial materials. A continuous search of stable and broad bandwidth SAs has been extensively carried out by the present researchers. Some of the promising materials that fit these criteria are nanomaterial media, such as carbon nanotubes (CNTs)[7] and graphene[8–12]. The low-loss CNT SA reported by Dong *et al.* successfully demonstrated *Q*-switched all-fiber lasers in the C-band region[13,14]. Two-dimensional materials of transition metal dichalcogenides (TMDs)[15,16] such as MoS_2 and WS_2 have also shown significant promise to become SA materials[17]. Most recently, black phosphorus (BP)[18] has drawn researchers' attention, as it may overcome several disadvantages of other materials. However, graphene has the drawback of having a very low modulation depth (typically <1% per layer)[19,20], while the CNT induces high losses due to broad tube diameter to cover broader bandwidth[21]. Due to the large bandgap in the visible region, TMDs have a limited performance in the near-infrared and mid-infrared regions[22]. Despite having a small and tunable bandgap by varying its film thickness, BP itself is environmentally unstable and tends to be easily damaged when exposed to oxygen and water molecules[23].

In recent years, quantum dot (QD) semiconductor nanocrystals have been discovered as a new class of nanomaterial SAs. QDs are zero-dimensional materials that have drawn a lot of attention in important applications, including SAs[24], laser power limiters, light-emitting diodes, optical switches, sensors[25–27], biological labeling, and solar cells. QDs have a small particle size that is between 1–100 nm with exceptional chemical processability. QD materials exhibit significant differences in their electronic and optical characteristics compared to bulk semiconductors due to the strong confinement of excited electrons and holes[28]. Normally, QD materials are doped in a glass material or poly-methyl-methacrylate (PMMA) via a thermal process. One QD material is CdSe, which has unique properties such as a stronger extinction coefficient, narrower band gap[29], higher quantum confinement effect, higher optical gain, broader absorption profile, better photochemical stability[30], and larger Stokes shift[30,31] compared to bulk semiconductors. A CdSe QD exhibits resonant non-linearity in slow times scales, which induces huge optical non-linearity, an important feature for generating *Q*-switched pulsed lasers[32]. The CdSe produced by the

QD method has significant advantages over other reinforcements due to the high surface area to volume ratio and the small size distribution. It contributes to high resistance to photobleaching and high photoluminescence efficiency[33]. Therefore, CdSe QD exhibits better Q-switched pulse stability for long-haul operations compared to other type of SAs, which makes it a promising candidate for high-performance and high durability SAs. So far, there has been no scientific report of using a CdSe QD as an SA to produce a Q-switched pulse based on an all-fiber laser. We demonstrate for the first time a CdSe QD passively Q-switched Yb-doped fiber laser (YDFL). The pump power variation of 975–1196 mW enable a repetition rate tuning range of 24.45–40.50 kHz at an optical wavelength of 1081 nm.

The synthesis process details are almost identical to those reported by Hamizi *et al.*[34]. It consists of CdO (99.99% purity), Se (99.99% purity), and manganese acetate (98%) powders as a precursor. For a surfactant and a solvent, oleic acid and paraffin oil are employed, respectively. First, we prepare the solvent by mixing oleic acid and paraffin oil in ratio of 3:5. By using a three-neck flask, the CdO, manganese acetate, and mixture of oleic acid and paraffin oil were mixed under an Ar flow at a temperature of 160°C and were stirred constantly until they completely dissolved. Subsequently, the solution was distilled in a vacuum to eradicate any remaining acetone. Next, the 0.16% Se powder was dissolved in paraffin oil at 220°C. Finally, the 5 mL Mn–Cd solution was swiftly added into the Se-paraffin oil solution, then exhibited rapid nucleation and gradual growth of the CdSe QD. The QD was then cleaned by a centrifugation process five times and washed in methanol to eradicate unreacted chemicals before being dried in a vacuum oven. Then, a CdSe QD powder was formed.

For the second phase, the CdSe QD powder was mixed with PMMA by an emulsion polymerization process[35]. The PMMA functions as a host material due to its characteristics of high optic transparency and low photoluminescent background[36]. First, about 4 mg of CdSe QD powder were added into 1 mL of PMMA, then it was dissolved as a solution. Concurrently, an emulsifier of 120 mg hexadecyltrimethylammonium bromide was dissolved in 8 mL of deionized water and then heated at 80°C. Next, this solution was stirred constantly while slowly adding the CdSe QD-PMMA solution. The resulting PMMA doped with CdSe QD was then deposited by centrifugation, drained with distilled water, and quickly sandwiched between two glass plates. The produced thin flake of PMMA-doped CdSe QD with a homogeneous surface on both sides is shown in Fig. 1(a). Surface homogeneity is very important for CdSe QD SA since an inhomogeneous surface will contribute to optical loss and pulse instability.

Transmission electron microscopy (TEM) samples were prepared by placing a drop of a diluted methanol suspension of CdSe QD on the surface of a mesh copper film, which was then dried for several days. Figure 1(b) shows the TEM images of the CdSe QD that were taken using

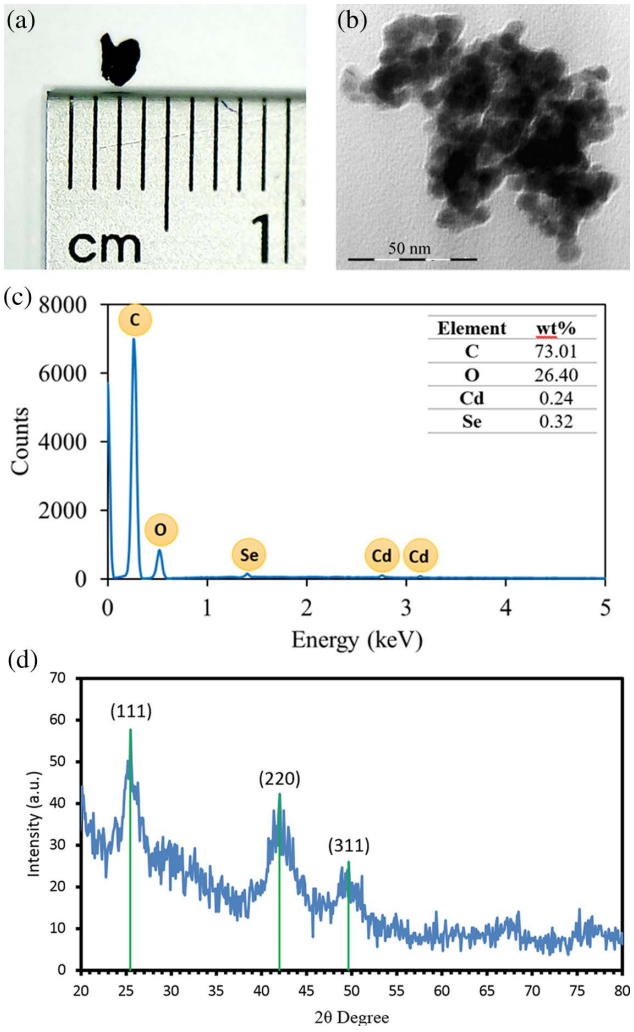

Fig. 1. PMMA doped with CdSe QD physical characteristics. (a) The end result of the CdSe QD thin flake. (b) The TEM micrograph and selected area electron diffraction pattern confirmed that the particle size is within the nanometer range, (c) The energy dispersive x ray spectroscopy measurement showing the existence of cadmium and selenide. (d) The XRD patterns of cubic crystalline CdSe QD.

LEO LIBRA 120 kV TEM. Notice that the individual CdSe particle diameter is approximately below 20 nm, which complies with the QD size requirement. Figure 1(c) shows the energy-dispersive x ray spectroscopy result that shows that the total concentration of CdSe is 0.56-wt. %, which is in range of normal doping concentrations. Very high presences of C and O are contributed by the PMMA, which has a composition of $C_5O_2H_8$. Figure 1(d) shows the x ray diffraction (XRD), which was obtained using a Siemens D500 x ray diffractometer consisting of graphite monochromatized Cu Kα radiation (0.15418 nm) irradiated with a scanning rate of 0.02 s^{-1}. The result obtained shows peaks around 2θ of 25.5°, 42°, and 49.7°, which correspond to the (111), (220), and (311) planes, respectively. These observed peaks satisfy the cubic crystal structure of CdSe that has lattice constants of 0.605 nm and is in good agreement with standard powder diffraction

data (JCPDS No. 65–2891 for CdSe, cubic)[37,38]. The broad peak of the XRD confirmed that the CdSe QD is nano-sized.

The experimental setup of using CdSe QD as an SA to produce a passively Q-switched YDFL is shown in Fig. 2. The setup used a 980 nm multimode laser diode (LD) pump that was connected to a multimode combiner (MMC), which provides the pump power to a gain medium of a 10 m double-clad Yb-doped fiber (YDF). The YDF has a numerical aperture of 0.46, a core radius of 5.5 μm, a cladding radius of 65 μm, and a cladding absorption of 3.9 dB/m at 975 nm. A 1 mm × 1 mm CdSe QD thin flake was sandwiched between 2 ceramic ferrules of fiber connectors adhered with an index matching gel, which forms a passive Q-switcher medium with an insertion loss of ~2.3 dB. The inset image shows the non-linear properties of CdSe. We radiate a mode-locked source into the CdSe sample, and the modulation depth of 11% was obtained. A polarization controller (PC) was employed to adjust the polarization state of the laser beam in the cavity[39]. The cavity output was split by 90/10 optical coupler (OC), which divides the output of 10% for the measurement of the spectrum, pulse, and power while the remaining 90% was fed back to the ring cavity and oscillated along the line. The output laser then connected to a 1.2 GHz InGaAs photodetector to convert the photon energy to an electrical signal, which was monitored by a 500 MHz oscilloscope and a 7.8 GHz radio-frequency (RF) spectrum analyzer. Additionally, the laser output was also measured by an optical spectrum analyzer with a spectral resolution of 0.05 nm and a digital power meter. The measured cavity length of the ring resonator was around 14.2 m.

In the experiment, the YDFL achieves a continuous-wave lasing threshold at a pump power of 850 mW.

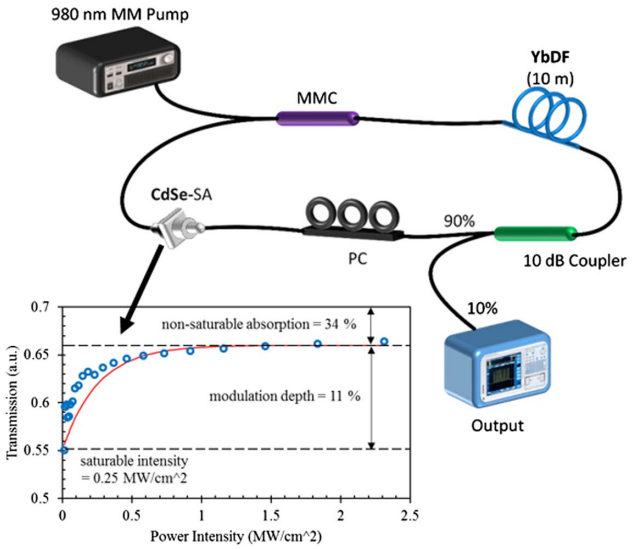

Fig. 2. Experimental setup of the proposed Q-switched YDFL employing a quantum-doped CdSe. Inset is non-linear properties of CdSe.

Subsequently, the laser changed its state to Q-switched at 975 mW, which the increased repetition rate observed when the pump power was increased up to 1196 mW, denoting a passive Q-switching operation. Figure 3(a) shows the optical spectrum of the resultant Q-switched pulses produced by the fiber laser at a pump power of 1196 mW, which produced a lasing wavelength of 1081 nm. The Q-switched pulse repetition rate was increased with the increased pump power, as shown in Fig. 3(b). This result proves that the Q-switched pulse can be tuned from 24.45 to 40.50 kHz by adjusting the pump power from 975 to 1196 mW. With the increased repetition rate, the pulse width narrowed from 6.78 to 3.65 μs. It was verified that the resulted pulse was only contributed by CdSe SA, since there no pulse trains were detected on the oscilloscope

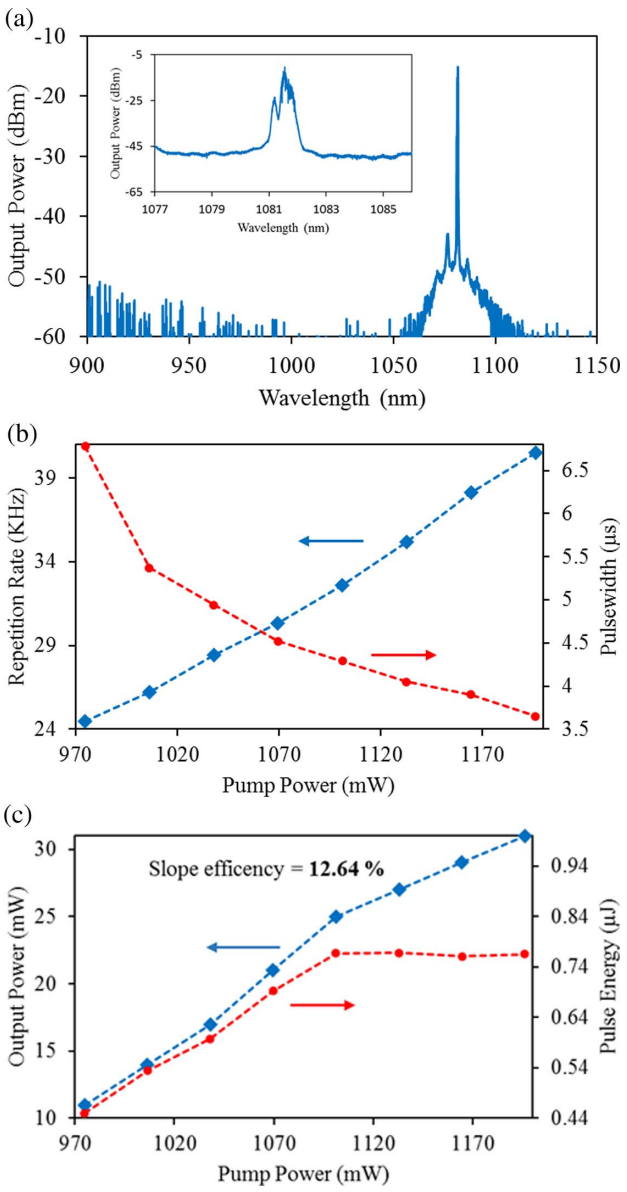

Fig. 3. Output characteristic of resultant Q-switched pulses. (a) Optical spectrum. (b) Repetition rate and pulse width versus pump power. (c) Output power and pulse energy versus pump power.

when the CdSe SA was removed, and the system operated under the all-normal cavity condition.

The laser threshold was high due to the long YDF used: it was 10 m. An extra-long YDF was employed to investigate the generation of pulses in 2-μm region. Managing group velocity dispersion (GVD) values in the cavity can narrow down the pulse width. The sign or value of the GVD is not the key to self-started pulsing; actually, it is a modulation depth of the SA[40]. Figure 3(c) shows the output power of the YDF laser and the calculated energy of a single pulse corresponding to the variation of power from 975 to 1196 mW. It was noted that the average output power is nearly linear with the increment of the input pump power when the maximum output power of 31 mW is recorded at pump power of 1196 mW. Based on the graph, the slope efficiency of the Q-switched laser was calculated at 12.64% when the maximum pulse energy was calculated at 0.77 μJ. It also revealed that the pulse energy was nearly linear with the pump power before the pump power reached 1101 mW. Then, the pulse energy was saturated and remained unchanged with the further increased pump power.

Figure 4 shows the pulse characteristics of the resulting Q-switched operation: the pulse waveform was well generated, as shown in Fig. 4(a). The generated pulse had a constant shape, frequency, and pulse width with no timing jitter presence. There was no trace of mode-locked pulses that may be generated due to the back-scattering effect. The light that propagates in the reverse direction through the 10 dB coupler and MMC will be weakened, which causes the back-scattering power to be dramatically reduced. In addition, the use of fusion splicing in all cavity connections also reduces the back-scattering effect. Figure 4(c) shows the RF spectrum of the Q-switched operation, in which the first spectrum emerges at a 40.50 kHz frequency and the second at an 81.00 kHz frequency, denoting a second harmonic. The spectrum continues to emerge over a span of 500 kHz frequency at a well composed harmonic frequency, which indicates a small pulse width. In addition, the signal-to-noise ratio was recorded at 42 dB, denoting Q-switched pulse and frequency stability.

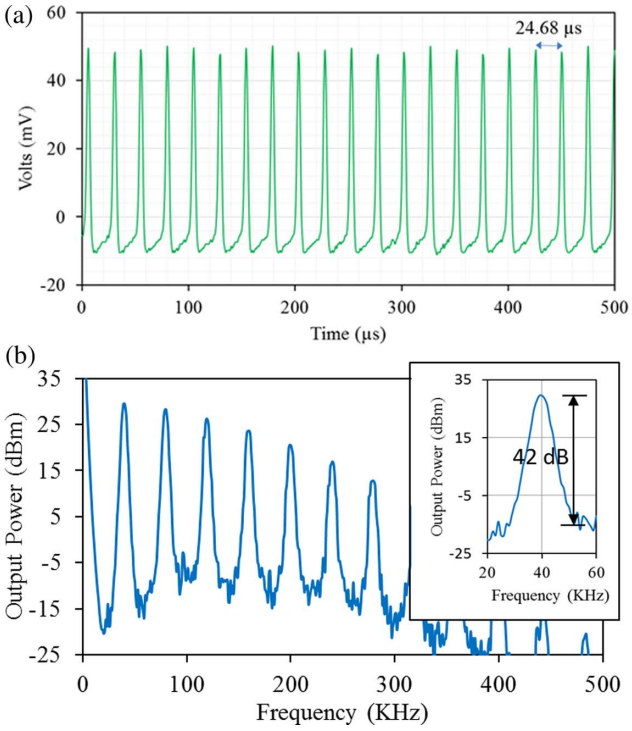

Fig. 4. Pulse characteristics of resulting Q-switched operation. (a) Pulse waveform. (b) RF spectrum.

We fabricate a new SA from PMMA-hosted CdSe QD and utilize it to generate a Q-switched pulse in a YDFL all-fiber configuration. The repetition rate is tunable from 24.45 to 40.50 kHz by varying the pump power from 975 to 1196 mW. Corresponding to these pump powers, the pulse width changes from 6.78 to 3.65 μs. The maximum calculated pulse energy is 0.77 μJ at pump power of 1101 mW. These overall results contribute to our work, which is dedicated to studying the optical and non-linear properties of CdSe QD, enhancing its potential for ultrafast photonics applications.

The authors would like to thank Ms. Ninik Irawati for her contributions and for sharing her knowledge on fabricating CdSe QDs.

References

1. M. E. Fermann and I. Hartl, Nat. Photon. **7**, 868 (2013).
2. N. Nishizawa, Jpn. J. Appl. Phys. **53**, 090101(1) (2014).
3. J. Philipps, T. Töpfer, H. Ebendorff-Heidepriem, D. Ehrt, R. Sauerbrey, and N. Borrelli, Appl. Phys. B **72**, 175 (2001).
4. J. Qiao, J. Zhao, K. Yang, S. Zhao, Y. Li, G. Li, D. Li, W. Qiao, T. Li, and H. Chu, Jpn. J. Appl. Phys. **54**, 032701(1) (2015).
5. W. Tian, C. Wang, G. Wang, S. Liu, and J. Liu, Laser Phys. Lett. **4**, 196 (2007).
6. S. Zhang, E. Wu, H. Pan, and H. Zeng, IEEE J. Quantum Electron. **40**, 505 (2004).
7. X. Xu, J. Zhai, L. Li, Y. Chen, Y. Yu, M. Zhang, S. Ruan, and Z. Tang, Sci. Rep. **4**, 6761 (2014).
8. Q. Bao, H. Zhang, Y. Wang, Z. Ni, Y. Yan, Z. X. Shen, K. P. Loh, and D. Y. Tang, Adv. Funct. Mater. **19**, 3077 (2009).
9. H. Zhang, D. Tang, R. Knize, L. Zhao, Q. Bao, and K. P. Loh, Appl. Phys. Lett. **96**, 111112 (2010).
10. J. Zhao, P. Yan, and S.-C. Ruan, Appl. Opt. **52**, 8465 (2013).
11. S. Huang, Y. Wang, P. Yan, G. Zhang, J. Zhao, H. Li, and R. Lin, Laser Phys. Lett. **11**, 025102 (2013).
12. S. Huang, Y. Wang, P. Yan, G. Zhang, J. Zhao, H. Li, and R. Lin, Laser Phys. **24**, 015001 (2013).
13. B. Dong, J. Hao, J. Hu, and C.-Y. Liaw, IEEE Photon. Technol. Lett. **22**, 1853 (2010).
14. B. Dong, J. Hu, C.-Y. Liaw, J. Hao, and C. Yu, Appl. Opt. **50**, 1442 (2011).
15. L. Mattheiss, Phys. Rev. B **8**, 3719 (1973).
16. Q. H. Wang, K. Kalantar-Zadeh, A. Kis, J. N. Coleman, and M. S. Strano, Nat. Nanotechnol. **7**, 699 (2012).
17. P. Yan, A. Liu, Y. Chen, H. Chen, S. Ruan, C. Guo, S. Chen, I. L. Li, H. Yang, and J. Hu, Opt. Mater. Express **5**, 479 (2015).
18. M. Hisyam, M. Rusdi, A. Latiff, and S. Harun, IEEE J. Sel. Top. Quantum Electron. 99 (2016).

19. S. D. D. D. Cafiso, E. Ugolotti, A. Schmidt, V. Petrov, U. Griebner, A. Agnesi, W. B. Cho, B. H. Jung, F. Rotermund, and S. Bae, Opt. Lett. **38**, 1745 (2013).
20. K. Janulewicz, A. Hapiddin, D. Joseph, K. Geckeler, J. Sung, and P. Nickles, Appl. Phys. A **117**, 1811 (2014).
21. W. Cho, J. Yim, S. Choi, S. Lee, A. Schmidt, G. Steinmeyer, U. Griebner, V. Petrov, D. I. Yeom, and K. Kim, Adv. Funct. Mater. **20**, 1937 (2010).
22. F. Bonaccorso and Z. Sun, Opt. Mater. Express **4**, 63 (2014).
23. J. O. Island, G. A. Steele, H. S. van der Zant, and A. Castellanos-Gomez, 2D Materials **2**, 011002 (2015).
24. A. M. Malyarevich, I. A. Denisov, V. G. Savitsky, K. V. Yumashev, and A. A. Lipovskii, Appl. Opt. **39**, 4345 (2000).
25. X. Peng, M. C. Schlamp, A. V. Kadavanich, and A. Alivisatos, J. Am. Chem. Soc. **119**, 7019 (1997).
26. D. Yang, Q. Chen, and S. Xu, J. Lumin. **126**, 853 (2007).
27. H.-W. Zan, C.-H. Li, C.-C. Yeh, M.-Z. Dai, H.-F. Meng, and C.-C. Tsai, Appl. Phys. Lett. **98**, 253503 (2011).
28. M. Green and P. O'Brien, Chem. Commun. **22**, 2235 (1999).
29. J. Zhu, O. Palchik, S. Chen, and A. Gedanken, J. Phys. Chem. B **104**, 7344 (2000).
30. P. Wang, Y. Wang, and L. Tong, Light: Sci. Appl. **2**, e102 (2013).
31. P. Jorge, M. A. Martins, T. Trindade, J. L. Santos, and F. Farahi, Sensors **7**, 3489 (2007).
32. J. Seo, S. Ma, Q. Yang, L. Creekmore, R. Battle, H. Brown, A. Jackson, T. Skyles, B. Tabibi, and W. Yu, in *Journal of Physics: Conference Series* (2006), 91.
33. R. Zhang, H. Yu, and B. Li, Nanoscale **4**, 5856 (2012).
34. N. A. Hamizi and M. R. Johan, Mater. Chem. Phys. **124**, 395 (2010).
35. A. DuChesne, A. Bojkova, J. Rottstegge, G. Glasser, D. Neher, and S. Krieger, Phys. Chem. Chem. Phys. **1**, 3871 (1999).
36. M. Artemyev and U. Woggon, Appl. Phys. Lett. **76**, 1353 (2000).
37. I. V. Lightcap, T. H. Kosel, and P. V. Kamat, Nano Lett. **10**, 577 (2010).
38. A. Raevskaya, A. Stroyuk, S. Y. Kuchmiy, Y. M. Azhniuk, V. Dzhagan, V. Yukhymchuk, and M. Y. Valakh, Colloids Surf. A: Physicochem. Eng. Aspects **290**, 304 (2006).
39. X. Peng, L. Manna, W. Yang, J. Wickham, E. Scher, A. Kadavanich, and A. P. Alivisatos, Nature **404**, 59 (2000).
40. R. Gumenyuk, I. Vartiainen, H. Tuovinen, and O. G. Okhotnikov, Opt. Lett. **36**, 609 (2011).